Xu et al. *Zool. Res.* 2022, 43(4): 552−565
https://doi.org/10.24272/j.issn.2095-8137.2022.031

ZR | Zoological Research

Article Open Access

DNA methylation-mediated expression of zinc finger protein 615 affects embryonic development in *Bombyx mori*

Guan-Feng Xu[1], Cheng-Cheng Gong[1], Yu-Lin Tian[1], Tong-Yu Fu[1], Yi-Guang Lin[1], Hao Lyu[1], Yu-Ling Peng[1], Chun-Mei Tong[1], Qi-Li Feng[1], Qi-Sheng Song[2], Si-Chun Zheng[1,*]

[1] *Guangdong Provincial Key Laboratory of Insect Developmental Biology and Applied Technology*, *Guangzhou Key Laboratory of Insect Development Regulation and Applied Research*, *Institute of Insect Science and Technology*, *School of Life Sciences*, *South China Normal University*, *Guangzhou*, *Guangdong* 510631, *China*

[2] *Division of Plant Science and Technology*, *College of Agriculture*, *Food and Natural Resources*, *University of Missouri*, *Columbia MO* 65211, *USA*

ABSTRACT

Cell division and differentiation after egg fertilization are critical steps in the development of embryos from single cells to multicellular individuals and are regulated by DNA methylation via its effects on gene expression. However, the mechanisms by which DNA methylation regulates these processes in insects remain unclear. Here, we studied the impacts of DNA methylation on early embryonic development in *Bombyx mori*. Genome methylation and transcriptome analysis of early embryos showed that DNA methylation events mainly occurred in the 5' region of protein metabolism-related genes. The transcription factor gene *zinc finger protein 615* (*ZnF615*) was methylated by DNA methyltransferase 1 (Dnmt1) to be up-regulated and bind to protein metabolism-related genes. *Dnmt1* RNA interference (RNAi) revealed that DNA methylation mainly regulated the expression of nonmethylated nutrient metabolism-related genes through *ZnF615*. The same sites in the *ZnF615* gene were methylated in ovaries and embryos. Knockout of *ZnF615* using CRISPR/Cas9 gene editing decreased the hatching rate and egg number to levels similar to that of *Dnmt1* knockout. Analysis of the *ZnF615* methylation rate revealed that the DNA methylation pattern in the parent ovary was maintained and doubled in the offspring embryo. Thus, Dnmt1-mediated intragenic DNA methylation of the transcription factor *ZnF615* enhances its expression to ensure ovarian and embryonic development.

Keywords: DNA methylation; Embryonic development; Transcriptional regulation; Epigenetic

INTRODUCTION

The zygote is the starting point of embryonic development. Embryogenesis is a complex process regulated by genetic and epigenetic mechanisms in which a zygote develops into a multicellular individual. DNA methylation via 5-methylcytosine (5mC), i.e., the covalent addition of a methyl (CH_3) group to the fifth carbon of the pyrimidine ring of cytosine residues of DNA molecules (Razin & Riggs, 1980; Yan et al., 2015), is an important epigenetic regulatory mechanism found in all

Received: 30 March 2022; Accepted: 24 May 2022; Online: 24 May 2022

Foundation items: This work was supported by the National Natural Science Foundation of China (31872286, 32100374)

*Corresponding author, E-mail: sczheng@scnu.edu.cn

species (Zilberman, 2008). In mammals, many genes in regions where DNA methylation occurs are involved in embryogenesis and early embryonic development (Slieker et al., 2015). In mouse embryos, DNA methylation defects can affect chromosome structure and histone modification levels, resulting in early embryonic death (Takebayashi et al., 2007). In cow embryos, the methylation dynamics of X-inactive specific transcript (XIST) are essential for the initiation of X chromosome inactivation, which affects embryonic development (Dos Santos Mendonça et al., 2019). In insects, DNA methylation is enriched in early embryos (Xu et al., 2022a). For example, 5mC deficiency in *Bombyx mori* causes ovarian dysplasia and embryonic lethality (Xiang et al., 2013; Xu et al., 2021), and silencing of DNA methyltransferase 1 (*Dnmt1*) in *Nasonia vitripennis* and *Blattella germanica* results in defective embryos (Ventós-Alfonso et al., 2020; Zwier et al., 2012). Therefore, DNA methylation is critical in animal embryogenesis.

In general, the establishment and maintenance of DNA methylation patterns are executed by an evolutionarily conserved family of DNA methyltransferases, including Dnmt3 (*de novo* DNA methyltransferase) and Dnmt1 (maintenance DNA methyltransferase) (Bird, 2002; Lister et al., 2009). Dnmt1 maintains pre-existing 5mC during DNA replication, while Dnmt3 is responsible for the generation of new 5mC sites (Glastad et al., 2011). In mammals, methylcytosine dioxygenase (TET3) is active, leading to low DNA methylation at the blastocyst stage, followed by Dnmt3a- and Dnmt3b-mediated *de novo* DNA methylation after blastocyst implantation (Greenberg & Bourc'his, 2019; Smith et al., 2014). In some insects, Dnmt3 is absent, and Dnmt1 is responsible for both *de novo* and maintenance DNA methylation (Falckenhayn et al., 2013; Lyko & Maleszka, 2011; Werren et al., 2010). However, the molecular and epigenetic mechanisms of Dnmt1 in the regulation of genomic DNA methylation in insect embryogenesis remain to be elucidated.

Many reports suggest that the mechanisms and patterns underlying genomic DNA methylation in insects differ from those in mammals (Glastad et al., 2011; Xiang et al., 2010; Xu et al., 2021; Zemach et al., 2010). In mammals, DNA methylation usually occurs in the promoter regions of target genes to create binding sites for specific transcription factors to activate the expression of tissue-specific genes or suppress the binding of transcription factors to promoters, resulting in altered transcriptional activity of the associated genes (Bird, 2002; Rishi et al., 2010; Zilberman, 2008). In mammalian cell nuclei, demethylation due to reprogramming (Byrne et al., 2003; Simonsson & Gurdon, 2004) up-regulates octamer-binding transcription factor 4 (*Oct4*) to ensure normal development of the embryo (Boiani et al., 2002; Bortvin et al., 2003). In insects, however, although DNA methylation in gene promoters regulates wing development through chitin metabolism (Xu et al., 2018, 2020), DNA methylation is enriched in gene bodies (Glastad et al., 2011; Xiang et al., 2010; Zemach et al., 2010). We previously found that intragenic DNA methylation recruits the acetylase Tip60 to enhance protein synthesis-related gene expression in the *B. mori* ovary (Xu et al., 2021).

In this study, we analyzed the methylome and role of *Dnmt1* in early embryos of *B. mori*, an economically valuable insect and model lepidopteran. We found that DNA methylation actively participated in embryogenesis by up-regulating the reproduction-specific transcription factor gene *zinc finger protein 615* (*ZnF615*) to enhance the expression of nutrient metabolism-related genes. Furthermore, the regulatory pathway was consistent between parent ovaries and offspring embryos.

MATERIALS AND METHODS

Insects and cell lines

The *B. mori* strain P50 was obtained from the Research and Development Center of the Sericulture Research Institute of Guangdong Academy of Agricultural Sciences, Guangdong, China. The moths were reared on fresh mulberry leaves at 27 °C under a 12 h light/12 h dark cycle.

The *B. mori* Bm12 (DZNU-Bm-12) cell line, originally derived from ovarian tissues (Khurad et al., 2009), was cultured at 28 °C in Grace's medium (Invitrogen, USA) supplemented with 10% fetal bovine serum (FBS) (HyClone, USA).

Dot blot assay

Genomic DNA was extracted from 50–60 silkworm embryos at each stage of embryonic development (i.e., fertilized egg, blastoderm, germ-band, organogenesis, reversal period, and head pigmentation) and digested with RNase A (Promega, USA) to eliminate RNA contamination. Genomic DNA (500 ng) was denatured at 95 °C for 10 min and immediately cooled on ice. The resulting genomic DNA was spotted on a nitrocellulose blot polyvinylidene fluoride (PVDF) membrane (GE Healthcare, China) and dried, followed by UV crosslinking for 1 min. The membrane was blocked with 3% (w/v) bovine serum albumin (BSA) in TBST (20 mmol/L Tris-HCl, 150 mmol/L sodium chloride, 0.05% Tween-20, pH 7.4) for 2 h at room temperature, then incubated with mouse anti-5mC antibody (1:1 000; ab10805, Abcam, UK) overnight at 4 °C. After three washes in TBST (10 min each), the membrane was incubated with horseradish peroxidase (HRP)-linked goat anti-mouse IgG secondary antibody (1:2 000; Dingguo Biotechnology, China) for 1.5 h at 37 °C. The input genomic DNA samples were spotted on the PVDF membrane, as indicated above, then directly stained with GoldView™ (Dingguo Biotechnology, China).

Whole-genome bisulfite sequencing (WGBS)

Genomic DNA was fragmented into 100–300 bp fragments by sonication, and a single "A" nucleotide was added to the 3' end of the blunt fragments. The fragments with the adapter were then bisulfite-converted using a Methylation-Gold Kit (Zymo, USA). Finally, the converted DNA fragments were amplified using polymerase chain reaction (PCR) and sequenced using the Illumina HiSeq™ 2500 platform by Gene Denovo Biotechnology Co. (China).

The obtained clean reads were mapped to the *B. mori* reference genome (Wang et al., 2005; Xia et al., 2004) using BSMAP (v2.90) (Xi & Li, 2009). The methylation level was

calculated based on the methylated cytosine percentages in the whole genome, in each chromosome, or in different regions of the genome for each sequence context (CG, CHG, and CHH). To assess differences in methylation patterns in different genomic regions, the methylation profiles in the flanking 2 kb regions and gene bodies (or transposable elements) were plotted based on the average methylation levels for each window.

RNA sequencing (RNA-seq) analysis

Total RNA from *B. mori* embryos was extracted using a TRIzol Reagent Kit (Invitrogen, USA) according to the manufacturer's protocols. RNA quality was assessed on an Agilent 2100 Bioanalyzer (Agilent Technologies, USA) and checked using electrophoresis on RNase-free agarose gel. RNA-seq was performed on the Illumina NovaSeq 6000 sequencing platform by Gene Denovo Biotechnology Co. (China). The raw reads were filtered to obtain clean reads, which were mapped to the *B. mori* reference genome (Wang et al., 2005; Xia et al., 2004) using HISAT2 v2.4 (Kim et al., 2015) with "RNA-strandness RF" and other parameters set to default. The assembled transcripts were generated after mapping, and their expression levels were normalized using FPKM values (fragments per kilobase of exon per million fragments mapped) by Cufflinks (Trapnell et al., 2012). Analysis of differentially expressed transcripts (DETs) between two groups was performed using DESeq2 software (Love et al., 2014). Transcripts with $P<0.05$ and absolute fold-change≥2 were considered DETs.

Western blotting

For western blot analysis, 40–100 μg of total protein extracted from embryos was separated using 10% sodium dodecyl sulfate-polyacrylamide gel electrophoresis (SDS-PAGE), followed by transfer to a nitrocellulose membrane (GE Healthcare, China). The membrane was blocked with 3% (w/v) BSA in TBST for 2 h at room temperature, followed by hybridization overnight at 4 °C in TBST containing 1% BSA and primary antibody (anti-Dnmt1 and anti ZnF 615). After washed in TBST three times, the membrane was then incubated with HRP-conjugated goat anti-rabbit/mouse IgG secondary antibody (1:2 000, Dingguo Biotechnology, China) for 2 h at 37 °C. Tubulin (Cat: TB002-R, Dingguo Biotechnology, China) was used as a reference to verify equal loading of the proteins on the gel.

Electrophoretic mobility shift assay (EMSA)

EMSA was conducted using a LightShift Chemiluminescent EMSA Kit (Thermo Scientific, USA). Methyl- or biotin-conjugated oligonucleotide probes were heated at 95 °C for 10 min and then slowly cooled to room temperature. Binding assays were performed according to the manufacturer's protocols. In brief, proteins were incubated for 20 min at room temperature with 20 μL of binding buffer (50 ng of poly(dI-dC), 2.5% glycerol, 0.05% NP-40, 50 mmol/L potassium chloride, 5 mmol/L magnesium chloride, 4 mmol/L EDTA, and 20 fmol of biotinylated end-labeled double-stranded probe). Different concentrations of unlabeled cold probes or unmethylated mutant probes were added to the binding mixture as competitors. After electrophoresis, the proteins were blotted onto positively charged nylon membranes (Hybond Nþ; Amersham Biosciences, UK), and the bands were visualized using the above EMSA kit according to the manufacturer's protocols.

CRISPR/Cas9 knockout of *Dnmt1* and *ZnF615*

Small guide RNA (sgRNA) sites on the exons of target genes were designed using CRISPRdirect (http://crispr.dbcls.jp/) (Naito et al., 2015) based on the GN19NGG motif. A pair of primers was synthesized to amplify the fragment containing the T7 promoter, target site, and gRNA sequences. The PCR product was purified and used as the template for transcription *in vitro*. The sgRNA was synthesized *in vitro* with the MEGAscript T7 Kit (Ambion, USA) following the manufacturer's instructions and then purified with sodium acetate/ethanol. The quality of the purified product was analyzed by gel electrophoresis.

The fertilized eggs were collected within 2 h after oviposition and immediately placed on a clean glass slide for injection. The sgRNA and Cas9 proteins were mixed to a final concentration of 800 ng/μL and 600 ng/μL, respectively. The mixture was injected into the eggs using a micromanipulator (Eppendorf FemtoJet 4i and 4r, Germany). To prevent contamination, the eggs were disinfected by steaming in 10% formaldehyde for 5 min and then placed in an incubator at 27 °C under a 12 h light/12 h dark cycle. All experimental operations were completed within 2 h of oviposition.

Identification of mutations at target sites

To confirm target gene mutation, the epidermis was collected for genomic DNA extraction when the silkworm larvae molted into pupae. Primers including regions upstream and downstream of the target sites were used for PCR to detect knockout of the target sequence. The PCR products were purified and ligated into the pMD-18T vector for sequencing.

Expression, purification, and antibody preparation of ZnF615 protein

The *ZnF615* open reading frame (ORF) (BGIBMGA007439) was cloned using cDNA from *B. mori* embryos with the primers shown in Supplementary Table S9. The cloned *ZnF615* cDNA was inserted into the pGEX-6P-1 vector with a GST tag at the N-terminus to generate an expression vector, which was then used to transform *Escherichia coli* (BL21) cells for protein expression. The recombinant protein was purified using a GST Protein Purification Kit according to the manufacturer's protocols (Beyotime, China) (Supplementary Figure S1). The purified recombinant GST-ZnF615 protein was mixed with Freund's adjuvant (Dingguo Biotechnology, China) and injected into BALB/c mice obtained from the Guangdong Medical Laboratory Animal Center (China). Antisera were collected after three booster injections, each with 100 μg of the recombinant protein.

Analysis of DNA affinity purification sequencing (DAP-seq)

DAP-seq was carried out using recombinant ZnF615 proteins. Genomic DNA extracted from silkworm embryos was sonicated to obtain fragments (~200 bp). The fragments were purified, end repaired, and ligated with Y-shaped adaptors, as

described previously (Bartlett et al., 2017), to generate a sequencing library for DAP-seq experiments. The ZnF615 ORF was inserted into the pFN19K-HALO plasmid to introduce a HaloTag at the N-terminus of the protein. The plasmid was transcribed and translated *in vitro* using TnT® SP6 High-Yield Wheat Germ Master Mix (Promega, USA). The subsequent steps were performed by Gene Denovo Biotechnology Co. (China) following standard DAP-seq protocols (Bartlett et al., 2017).

The DAP-seq reads were mapped to the *B. mori* reference genome (Wang et al., 2005; Xia et al., 2004) using Bowtie2 (v2.2.5) (Langmead & Salzberg, 2012). All reads from the interval, 2 kb region upstream of the transcriptional start site (TSS), and 2 kb region downstream of the transcriptional termination site (TTS) were counted using deepTools (v3.2.0) (Ramírez et al., 2016). MACS2 (v2.1.2) (Zhang et al., 2008) was used to identify read-enriched regions from the DAP-seq data. Dynamic Poisson distribution was used to calculate the *P*-value of the specific region based on the unique mapped reads. The region was defined as a peak when the *q*-value was <0.05. Peak-related genes were annotated using the ChIPseeker package in R (Yu et al., 2015). Based on genomic location and gene annotation information of the peaks in the *B. mori* reference genome, peak-related genes and their distributions in different regions (e.g., intergenic, intron, downstream, upstream, and exon regions) were identified. MEME (v5.4.1) (http://meme-suite.org/tools/meme) and DREME (v5.4.1) (http://memesuite.org/tools/dreme) were used to detect specific motifs.

Quantitative real-time PCR (qRT-PCR)

Total RNA was extracted using TRIzol (TaKaRa, Dalian, China), and cDNA was synthesized using a First-Strand cDNA Synthesis Kit (TaKaRa, Dalian, China). QRT-PCR was performed using a 2×SYBR PremixEXTaq^{TM} Kit (TaKaRa, China). Relative gene expression level was calculated using the $2^{-\Delta\Delta Ct}$ method (Livak & Schmittgen, 2001). Data were normalized to the housekeeping gene ribosomal protein 49 (*Rp49*). All data represent three biological replicates and three technical repeats.

Construction of luciferase vector

Genomic DNA was extracted from the *B. mori* embryos. The promoter of the *actin* gene, including the 365 bp core promoter and 63 bp 5' untranslated region (UTR), was cloned into the pMD-18T vector (TaKaRa, Dalian, China). The promoter and gene body of the *ZnF615* gene were amplified by PCR and then cloned into the luciferase reporter vector pGL3-basic (Promega, USA).

RNA interference (RNAi)

For RNAi in the *B. mori* embryos, a 200–600 bp unique fragment of the target gene ORF was chosen as the template for the synthesis of gene-specific double-stranded RNA (dsRNA) using the T7 RiboMAX^{TM} Express RNAi System (Promega, USA). The synthesized dsRNA (20–50 ng) was injected into embryos within 2 h of oviposition using a micromanipulator, as described previously (Xu et al., 2022b). Three replicates consisting of 300–400 embryos per replicate were carried out. To evaluate knockdown efficiency, qRT-PCR was performed using the specific primers.

Analysis of egg number and hatch rate

To record egg number, ovaries were dissected from wild-type (WT), *Dnmt1*$^{-/-}$, and *ZnF615*$^{-/-}$ *B. mori* moths daily from the first to eighth day of the pupal stage, and the eggs in the dissected ovaries were collected and counted.

The larvae hatched from the eggs were recorded on days 6–10.5 after oviposition. The hatch rate was calculated as: hatch rate=number of larvae/number of eggs.

Statistical analysis

For all measurements, data are presented as the mean±standard error (*SE*). *P*-values for group comparisons were calculated using a paired Student's *t*-test (*: $P<0.05$; **: $P<0.01$; ***: $P<0.001$).

RESULTS

***Dnmt1* knockout suppresses embryogenesis**

Previous research has shown that *Dnmt1* knockdown by RNAi impacts embryonic development in *B. mori* (Xiang et al., 2013; Xu et al., 2021). To confirm this result, CRISPR/Cas9 gene editing was applied to knockout the *Dnmt1* gene. First, sgRNAs targeting *Dnmt1* exon 4 were injected into *B. mori* embryos within 2 h of oviposition. The knockout mutants were detected by aligning the edited target sequences to the WT genomic sequences. One mutant showed a deletion of 52 bases in *Dnmt1* exon 4 (Figure 1A), resulting in a defective protein of only 203 amino acids without functional domains, significantly different from the complete Dnmt1 protein of 1 409 amino acids (Figure 1B). The hatching rate in the *Dnmt1*$^{-/-}$ group was only 38.09%, a decrease of 57.66% from the WT group, which had a 95.75% hatching rate at days 10–11 (Figure 1C). Western blot analysis showed that both *Dnmt1*$^{-/-}$ hatched and *Dnmt1*$^{-/-}$ unhatched embryos lacked a complete Dnmt1 protein (Supplementary Figure S2). At day 8 post-oviposition, defects in the unhatched *Dnmt1*$^{-/-}$ embryos were found, whereas the WT embryos had developed and started to hatch. The head, thorax, abdomen, gut, and leg segments of the mutant were underdeveloped, suggesting that early development was affected by *Dnmt* knockout (Figure 1D). Ovarian development was also altered in the *Dnmt1*$^{+/-}$ heterozygotes compared to the WT. The egg number generated by *Dnmt1*$^{+/-}$ decreased by approximately 20% compared to the WT (Supplementary Figure S3). These results indicate that DNA methylation catalyzed by Dnmt1 has a considerable influence on ovarian development and early embryogenesis.

Identification of DNA-methylated genes required for embryogenesis

To study how DNA methylation affects embryonic development, 5mC levels in embryos at different developmental stages were examined by qRT-PCR and dot blot analysis. Results showed that 5mC was detectable throughout embryonic development but was higher during the early embryonic stages (i.e., fertilized egg, blastoderm, and germ-band) than during the late embryonic stages (i.e., organogenesis, reversal period, and head pigmentation)

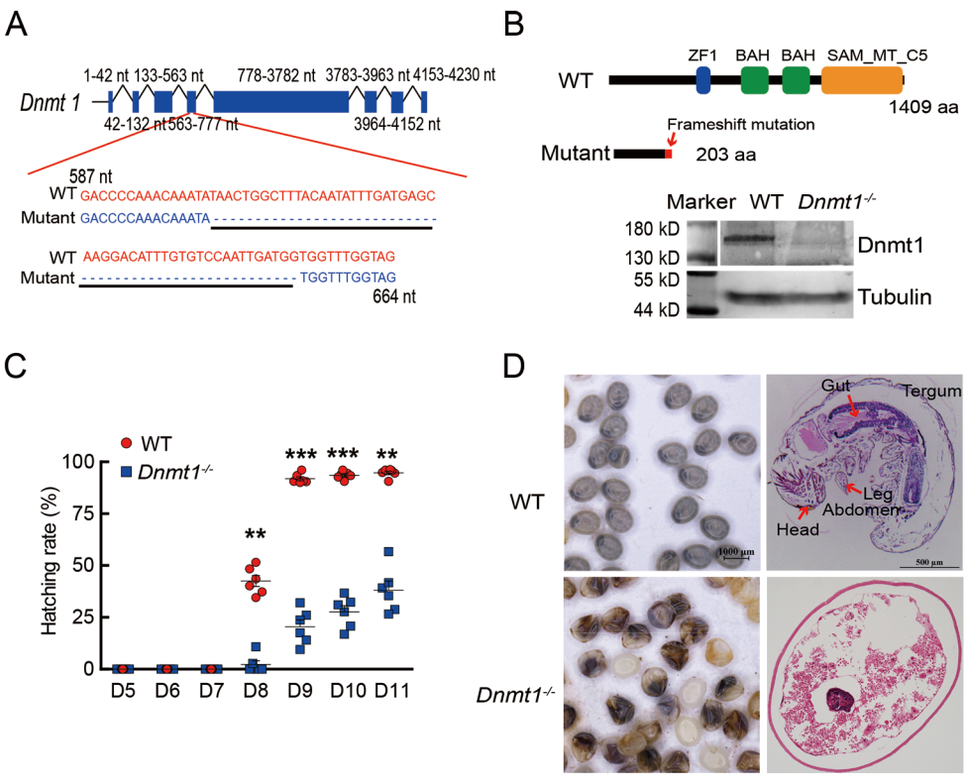

Figure 1 Effect of *Dnmt1* knockout on embryonic development and egg hatching in *B. mori*

A: Schematic of nucleic acid base deletion site in *Dnmt1*. B: Functional domain (top) and western blot (bottom) analysis of Dnmt1 protein in wild-type (WT) and *Dnmt1*$^{-/-}$ mutant. C: Changes in hatching rate of WT and *Dnmt1*$^{-/-}$ mutant. Each point represents the embryo hatching rate of female WT or *Dnmt1*$^{-/-}$ silkworms. D: Morphology and structure of WT and *Dnmt1*$^{-/-}$ embryos. Significant differences were determined by *t*-test (*: $P<0.05$; **:$P<0.01$; ***: $P<0.001$).

(Figure 2A). Illumina WGBS of genomic DNA from blastoderm-stage embryos, when the highest *Dnmt1* mRNA level was detected (Figure 2A), showed a total of 439 751 5mCs in the whole genome, representing 0.67% of all cytosine sites in the *B. mori* genome (Figure 2B; Supplementary Table S1). CG methylation (70.92%) was higher than CHG (4.99%) and CHH (24.09%) methylation (H represents A, C, or T). CG, CHG, and CHH methylation occurred at 1.34%, 0.44%, and 0.50% of the genome-wide CG, CHG, and CHH sites, respectively. In the CG context, DNA methylation occurred predominantly in gene bodies, particularly in the exons (Figure 2B). Gene annotation showed that the methylated genes were mainly enriched in pathways related to protein metabolism, including ribosome, ribosome biogenesis in eukaryotes, proteasome, aminoacyl-tRNA biosynthesis, protein processing in endoplasmic reticulum (ER), ubiquitin-mediated proteolysis, and protein export (Supplementary Figure S4). In addition, four groups of genes were identified according to mean expression levels. The relationship between the expression levels of these genes and DNA methylation rates was analyzed (Figure 2C). Most methylation changes in the genes occurred around the TSSs. The gene expression levels were positively correlated with the methylation rates (Figure 2C), suggesting that the methylated protein metabolism-related genes were expressed at high levels, whereas unmethylated genes were expressed at low levels.

To further investigate the transcription products of the target genes of DNA methylation, RNA-seq was implemented after *Dnmt1* RNAi. The fertilized zygotes were injected with *dsgfp* (control) or *dsDnmt1* and collected after 48 h to evaluate RNAi efficiency and conduct RNA-seq. The *Dnmt1* mRNA level was significantly decreased by RNAi (Supplementary Figure S5). Transcriptome data showed that 24 up-regulated genes and 105 down-regulated genes were identified between the *Dnmt1* RNAi treatment and control (Figure 2D; Supplementary Table S2). Differentially expressed genes (DEGs) were mainly enriched in nutrient metabolic pathways, including lipid, amino acid, and carbohydrate metabolism (Figure 2E). Among the 129 DEGs, 23 had a methylation rate of more than 0.5% (Figure 2D), which may be positively correlated with the mRNA level. Among these 23 DEGs, the mCpG sites of 20 genes were enriched around their TSSs (Supplementary Figure S6 and Table S3). To investigate whether *Dnmt1* RNAi affects embryogenesis through these 23 genes, their expression patterns were compared with that of *Dnmt1* from the fertilized egg to head pigmentation stages of embryonic development via the transcriptome (Xu et al., 2022a). Four genes (*BGIBMGA007439*, *BGIBMGA005446*, *BGIBMGA012542*, and *BGIBMGA006364*) were found to have identical expression patterns to *Dnmt1* (Figure 2F; Supplementary Table S4), implying that they may be positively regulated by DNA methylation. Therefore, these four genes were selected as target genes of *Dnmt1* for further study.

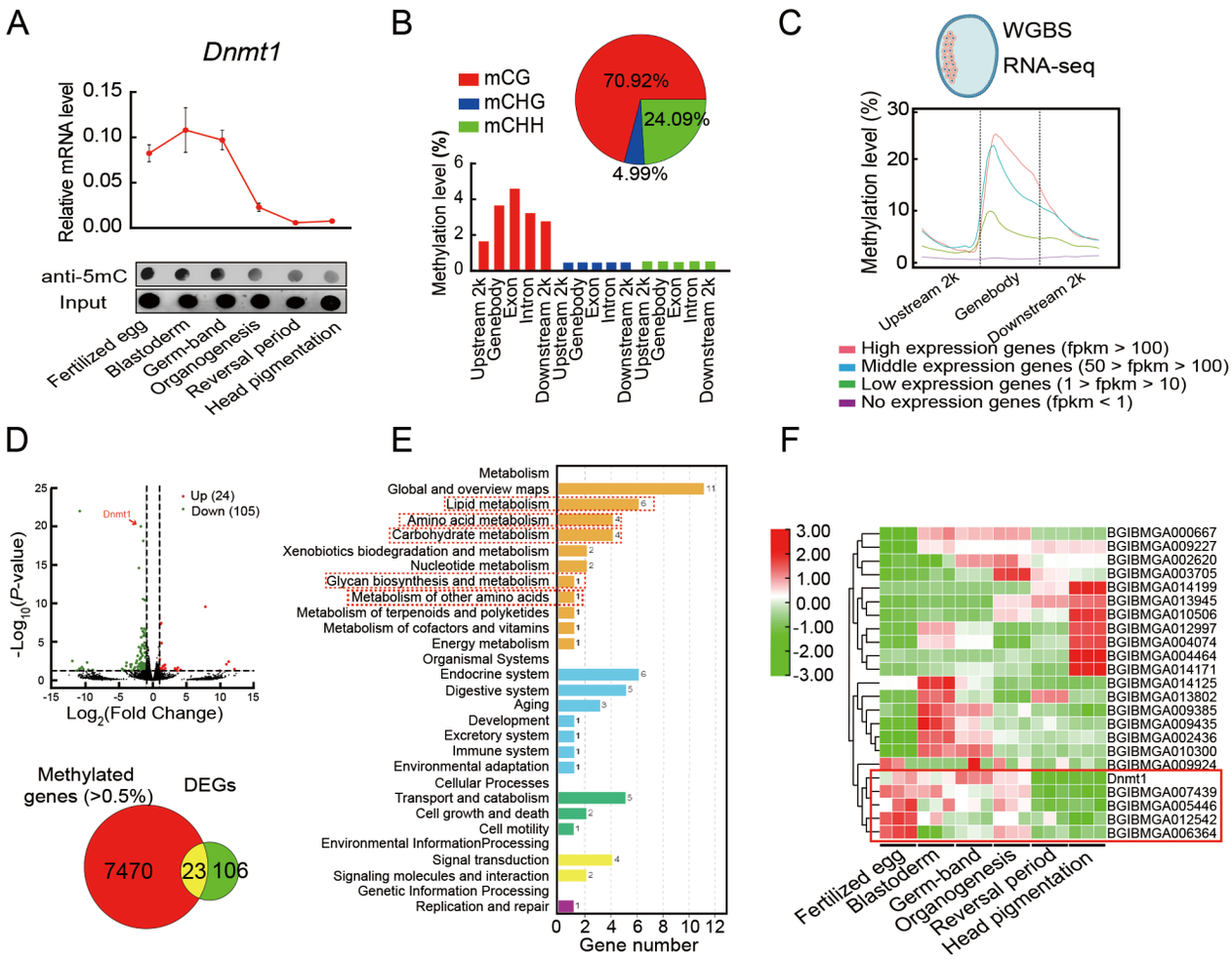

Figure 2 Identification of DNA methylation-modified genes affecting embryonic development in *B. mori*

A: qRT-PCR (top) and dot blot (bottom) analyses of methyltransferase (*Dnmt1*) expression levels and 5mC levels at six different embryonic development stages. B: Distribution of mC methylation in CG, CHG, and CHH contexts (H represents A, C, or T) in different gene regions (gene body, exon, intron, and 2 kb upstream and downstream of gene body). C: mCG levels in genes with different expression levels. Genes were classified into four groups based on mean expression levels (High expression: FPKM>100; Middle expression: 10<FPKM≤100; Low expression: FPKM<10; No expression: FPKM<1). D: Volcano plot analysis of differentially expressed genes (DEGs) after *Dnmt1* RNAi at blastoderm stage (top). Venn diagram comparing DEGs identified by RNA-seq after *Dnmt1* RNAi and methylation genes identified by WGBS in embryos (bottom). E: KEGG analysis of DEGs after *Dnmt1* RNAi in *B. mori* embryos. F: Hierarchical clustering heat map of *Dnmt1* and 23 genes both methylated and differentially expressed in (D) during the six different stages of embryo development (fertilized egg, blastoderm, germ-band, organogenesis, reversal period, and head pigmentation).

To determine the roles of these candidate genes in embryogenesis, dsRNA targeting *BGIBMGA007439*, *BGIBMGA005446*, *BGIBMGA012542*, and *BGIBMGA006364* was injected into eggs on the first day of oviposition (Supplementary Figure S7). Knockdown of the *BGIBMGA007439* gene, corresponding to the zinc finger protein ZnF615 containing six zinc finger motifs and a zinc finger associated domain (Figure 3A), significantly reduced the hatching rate (Figure 3B), whereas RNAi of the other three candidate genes did not have an obvious effect on hatching (Supplementary Figure S8). Furthermore, the mRNA (Figure 3C) and methylation levels (Figure 3D) of the promoter and gene body of *ZnF615* were significantly decreased after *Dnmt1* RNAi, indicating that *ZnF615* is downstream of *Dnmt1* and involved in embryogenesis.

DNA methylation in *ZnF615* gene body enhances its expression

To investigate how 5mCG is involved in *ZnF615* expression, eight 100 bp regions that showed the largest differences in mCG levels in the promoter (regions 1–4) or gene body (regions 5–8) of *ZnF615* after *Dnmt1* RNAi were selected and analyzed to determine their regulatory activities using a luciferase assay (Figure 4A; Supplementary Figure S9). The transcriptional activity of the luciferase reporter under the control of the individual regions fused with the core promoter of the *actin* gene was tested in *Bm*12 cells with *Dnmt1* RNAi (Supplementary Table S5). The transcriptional activities of regions 5 and 7 in the gene body were significantly inhibited

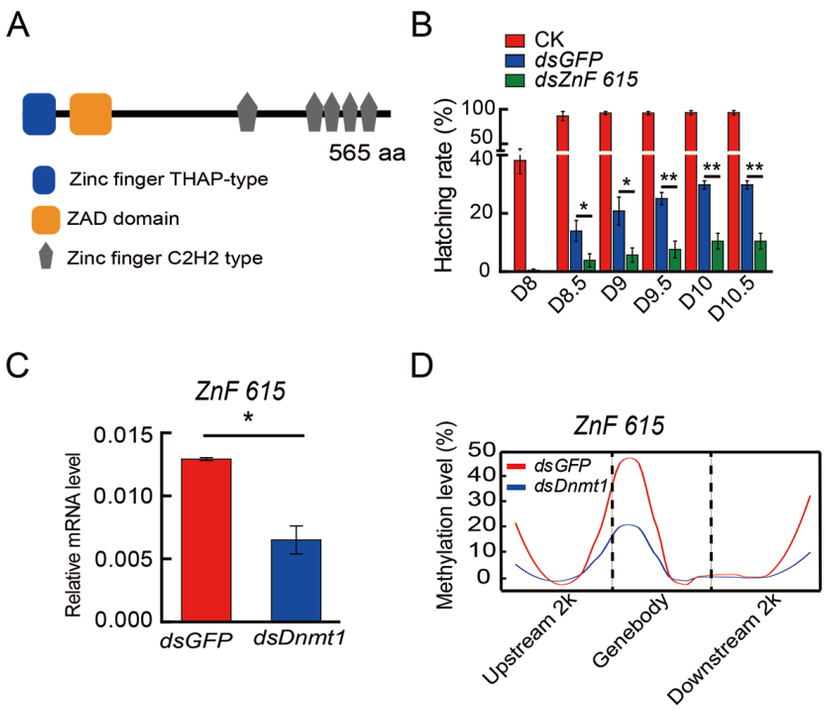

Figure 3 DNA methylation of *ZnF615* by Dnmt1 affects *B. mori* embryonic development

A: Analysis of functional domain of ZnF615 protein. B: Changes in hatching rate after *ZnF615* dsRNA treatment. dsRNA was injected into *B. mori* embryos within 2 h post-oviposition. Dn: n-Day of embryonic development. C: Change in *ZnF615* mRNA levels after *Dnmt1* RNAi in *B. mori* embryos. D: Changes in mCG levels in upstream 2 kb, gene body, and downstream 2 kb regions of *ZnF615* gene in *B. mori* embryos after *Dnmt1* RNAi. Significant differences were determined by *t*-test (*: P<0.05; **: P<0.01).

by *Dnmt1* RNAi, whereas that of region 6 was enhanced. The transcriptional activities of regions 1 and 4 in the promoter were also regulated by *Dnmt1* RNAi, but activity was extremely low (Figure 4B). Mutations in regions 5 and 7, in which CG at the mCpG sites was replaced by AT (Supplementary Figure S9), did not cause any change in transcriptional activity after *Dnmt1* RNAi (Figure 4C). Thus, we assume that 5mC in the gene body rather than in the promoter of the *ZnF615* gene is primarily responsible for regulation of gene expression. These results indicate that methylation in regions 5 and 7 in the gene body enhances *ZnF615* gene expression, which offsets the inhibitory effect of region 6 during embryogenesis in silkworms.

To confirm whether *Dnmt1* directly binds to regions 5 and 7 in the gene body, thereby catalyzing the formation of mCG, EMSA was conducted with the biotin-labeled region 5 or 7 probes and nuclear proteins isolated from silkworm embryos (Figure 5). Nuclear proteins bound to labeled region 5 or 7 probes could be competed off with 50× or 100× nonlabeled probes (cold probe) but not with mutated nonlabeled probes (Figure 5A, B). To confirm whether the binding protein is Dnmt1, a supershift assay was performed using an anti-Dnmt1 antibody (Xu et al., 2021). A supershifted band was detected when the anti-Dnmt1 antibody was present (Figure 5C), suggesting that the protein bound to the of region 5 or 7 probes was Dnmt1. Thus, the transcriptional activity assay and EMSA results demonstrated that DNA methylation catalyzed by Dnmt1 in gene body regions promoted *ZnF615* expression.

Knockout of *ZnF615* suppresses embryogenesis

To confirm the function of *ZnF615* in embryogenesis, CRISPR/Cas9 gene editing was applied to knockout the *ZnF615* gene. The qRT-PCR results showed that *Dnmt1* and *ZnF615* had similar expression patterns, with higher mRNA levels in embryos and gonads at the pupal stages in the WT silkworms (Figure 6A). A *ZnF615* mutant, in which two bases in exon 4 were deleted (Figure 6B), formed a defective protein of 205 amino acids, lacking five of the zinc finger motifs in the complete protein of 565 amino acids (Figure 6C), and the full-length ZnF615 protein could barely be detected in *ZnF615*$^{-/-}$ (Figure 6D top). The hatching rate in the homozygous *ZnF615*$^{-/-}$ mutant was similar to that in the *Dnmt1*$^{-/-}$ mutant (Figure 6D bottom), and the embryos were unable to develop normally, with only 53.54% of the eggs hatching (Figure 6D bottom). Similar to *Dnmt1*$^{-/-}$ *B. mori*, both *ZnF615*$^{-/-}$ hatched and *ZnF615*$^{-/-}$ unhatched embryos lacked the complete ZnF615 protein (Supplementary Figure S10).

Paraffin sections of *ZnF615*$^{-/-}$ mutant embryos at day 8 post-oviposition revealed that the unhatched *ZnF615*$^{-/-}$ embryos did not undergo complete embryogenesis and the organs were undifferentiated and unformed at the early stage (Figure 6E). Some of the hatched *ZnF615*$^{-/-}$ silkworms also died during the larval period, although about 30% survived to adulthood (Figure 6E). However, the *ZnF615*$^{+/-}$ embryos hatched and developed normally (Supplementary Figure S11). This phenotype was similar to that of the *Dnmt1*$^{-/-}$ mutant. In addition to the low hatching rate, egg number in the *ZnF615*$^{-/-}$ mutant decreased by approximately 20% compared to the WT

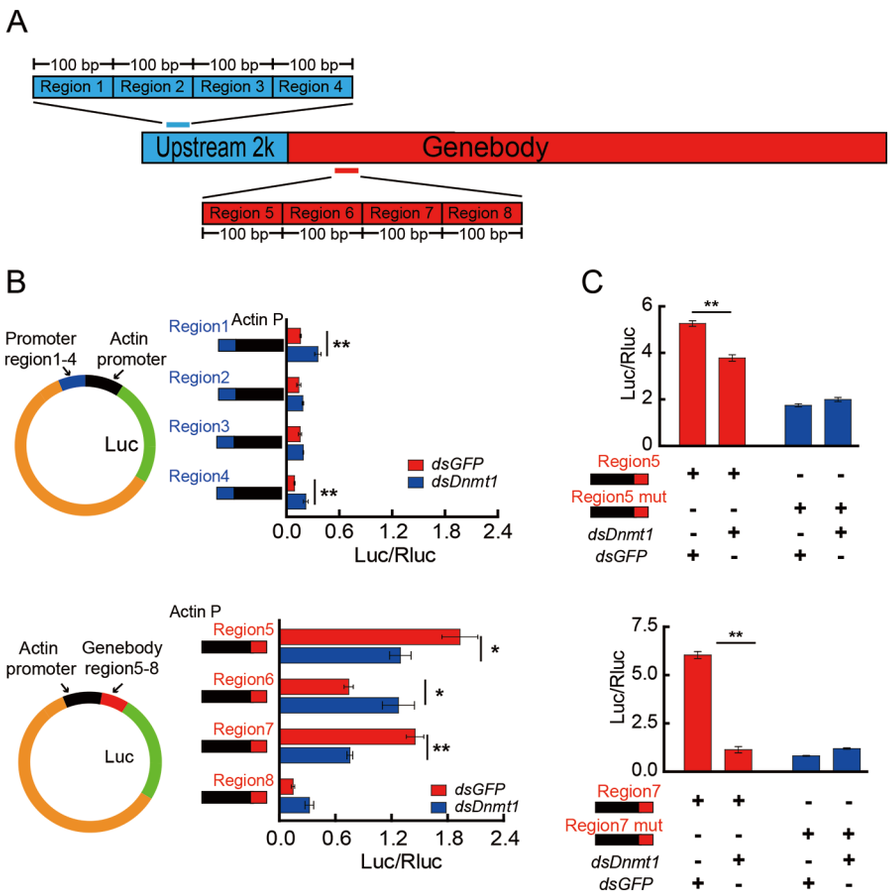

Figure 4 Effect of DNA methylation in promoter and gene body on transcription of *ZnF615* gene

A: Schematic of eight 100 bp fragments with the largest differences in mCG levels in promoter and gene body of *ZnF615* gene after *Dnmt1* RNAi. B: Effects of different promoter (top) and gene body (bottom) regions on luciferase activity. Different regions (regions 1–4) of promoter fragments were inserted upstream of the actin promoter and luciferase ORF. Different regions (regions 5–8) of the gene body were constructed into the luciferase vector between the actin promoter and luciferase ORF. C: Changes in activity of luciferase reporters containing WT or cytosine-mutated region 5 (top) or 8 (bottom) of the gene body of *ZnF615* in *Bm*12 cells co-transfected with *dsDnmt1* or *dsGFP*. Significant differences were determined by *t*-test (*: $P<0.05$; **: $P<0.01$).

(Supplementary Figure S12).

Identification of genes required for embryogenesis regulated by DNA methylation-mediated ZnF615

To determine which downstream target genes are regulated by ZnF615, DAP-seq analysis was carried out. Immunofluorescence assays showed that the ZnF615 protein was localized to the nucleus of *Bm*12 cells (Supplementary Figure S13), implying that it is a nuclear factor acting on its target genes. Therefore, we used DAP-seq to identify the target genes acted upon by *ZnF615* in the silkworm genome (Figure 7A). By mapping the DAP-seq reads to the *B. mori* genome, ZnF615 binding sites and motifs were identified (Figure 7A). ZnF615 had binding sites on each scaffold, especially high peak number regions on Ps01–06 (Supplementary Figure S14). The ZnF615 binding sites were enriched in the regions near the TSS and TTS (Figure 7B). The most frequently appearing sequence motif was TTTTTATTTGTTTTT (Figure 7C), suggesting that this may be the specific motif for ZnF615 binding. A total of 1 209 ZnF615 candidate binding genes were annotated (Supplementary Table S6). To further investigate the genes regulated by DNA methylation-mediated ZnF615, we combined the ZnF615 peak-related genes from DAP-seq and DEGs identified by RNA-seq after *Dnmt1* RNAi (Figure 7D). Nine DEGs after *Dnmt1* RNAi were enriched in ZnF615 DAP-seq (Supplementary Table S7). The mRNA levels of these nine genes were determined by qRT-PCR after *ZnF615* RNAi, with six showing significant reductions (Figure 7D), i.e., adhesive plaque matrix protein, synaptic vesicle glycoprotein 2B, uncharacterized protein LOC101738308, cuticular protein glycine-rich 19, obscurin, and AGAP005312-PA-like protein (Supplementary Figure S15). These findings suggest that the genes directly bound by ZnF615 and down-regulated by *Dnmt1* RNAi are not nutrient metabolism-related genes. Therefore, in the *ZnF615*-knockdown embryos, we detected changes in the expression of nutrient metabolism-related DEGs enriched after *Dnmt1* RNAi, including amino acid, carbohydrate, and lipid metabolism pathways (Figure 7E; Supplementary Table S8). The qRT-PCR results showed that nine of the 13 nutrient metabolism-related genes enriched by

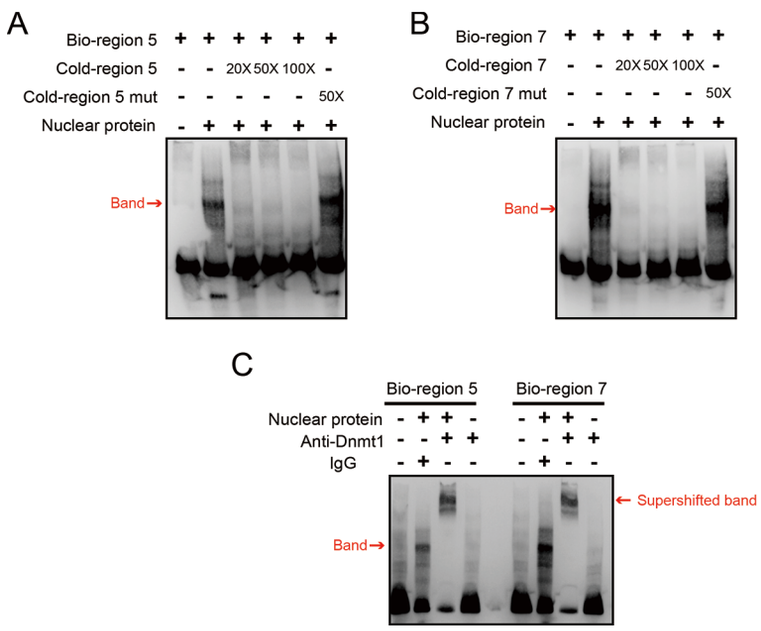

Figure 5 EMSA analysis of Dnmt1 binding with regions 5 and 7 in *ZnF615* gene body

A: Binding of nuclear proteins isolated from *B. mori* embryos with region 5 probe. B: Binding of nuclear proteins isolated from *B. mori* embryos with region 7 probe. Cold probe is unlabeled region 5 or 7 oligos. C: Supershifted band was detected using anti-Dnmt1 antibody. IgG was used as a negative control. Sequences of WT and mutant region 5 and 7 probes are shown in Supplementary Table S9.

Dnmt1 RNAi were significantly decreased after *ZnF615* RNAi (Figure 7E), including lipase, glucose dehydrogenase, and glucosidase metabolism-related genes. These results indicate that DNA methylation may enhance the expression of these genes via its effects on ZnF615.

As Dnmt1-mediated ZnF615 methylation affects the development of embryos and ovaries, we further investigated whether ZnF615 is methylated at the same sites and at the same level in the ovary and embryo. Analysis showed that the methylation regions in the *ZnF615* gene were similar between the ovary and embryo, but the methylation level of the *ZnF615* gene in the embryos was twice that in the ovaries (Figure 7F) (Xu et al., 2021). These observations suggest that DNA methylation of the *ZnF615* gene is involved in the regulation of early embryogenesis in *B. mori* and that modification of *ZnF615* methylation in the embryos likely originates in the ovaries and is strengthened by *Dnmt1* activity during embryogenesis.

DISCUSSION

Properly regulated gene expression is essential for embryonic development. In *B. mori*, the fertilized zygote progresses through the blastoderm, germ-band, organogenesis, reversal period, and head pigmentation stages to develop into a mature embryo. Many genes related to DNA replication, transcription, protein synthesis, and epigenetic modifications are up-regulated before embryonic organogenesis, while genes related to hormone synthesis and signaling, neuropeptides, and cuticle proteins are up-regulated at or after the organogenesis stage (Xu et al., 2022a). Thus, DNA methylation modifications may regulate early embryonic development by influencing the expression of genes necessary for cell division and differentiation. DNA methylation is associated with embryonic development in hemimetabolous and holometabolous insects (Bewick et al., 2019; Li et al., 2020; Ventós-Alfonso et al., 2020; Xiang et al., 2013). However, how DNA methylation affects insect embryonic development remains unclear. In this study, we confirmed the critical role of DNA methylation in *B. mori* embryogenesis by *Dnmt1* knockout (Figure 1). We found that DNA methylation level was higher in early embryogenesis than in later embryogenesis (Figures 1, 2A). Based on genome-wide methylation analysis in early embryos, we also found that 5mC methylation mainly occurred in the gene bodies of highly expressed protein metabolism-related genes (Figure 2C; Supplementary Figure S4) required for early embryonic development. We determined that the nuclear protein ZnF615 gene was downstream of *Dnmt1* (Figure 3). Finally, we revealed that the expression of nutrient metabolism-related genes was inhibited by *Dnmt1* and *ZnF615* RNAi (Figures 2E, 7D, E). Based on these findings, we hypothesize that downstream genes regulated by Dnmt1-induced *ZnF615* methylation are vital for early *B. mori* embryonic development.

Research has reported that 5mC affects early embryonic development in insects. In *Tribolium castaneum*, DNA methylation occurs in the early stage of embryogenesis, followed by global demethylation as the embryo develops (Feliciello et al., 2013). *Dnmt1* RNAi in *B. germanica*, which has both *Dnmt1* and *Dnmt3*, results in defective embryos (Ventós-Alfonso et al., 2020). In this study, we demonstrated that knockout of *Dnmt1*, the only DNA methyltransferase in *B. mori*, stopped early embryonic development and even induced death (Figure 1), similar to that of *Dnmt1* RNAi (Lyu et al., 2021; Xiang et al., 2013; Xu et al., 2021). However, nearly 40% of the homozygous knockout mutants hatched and grew

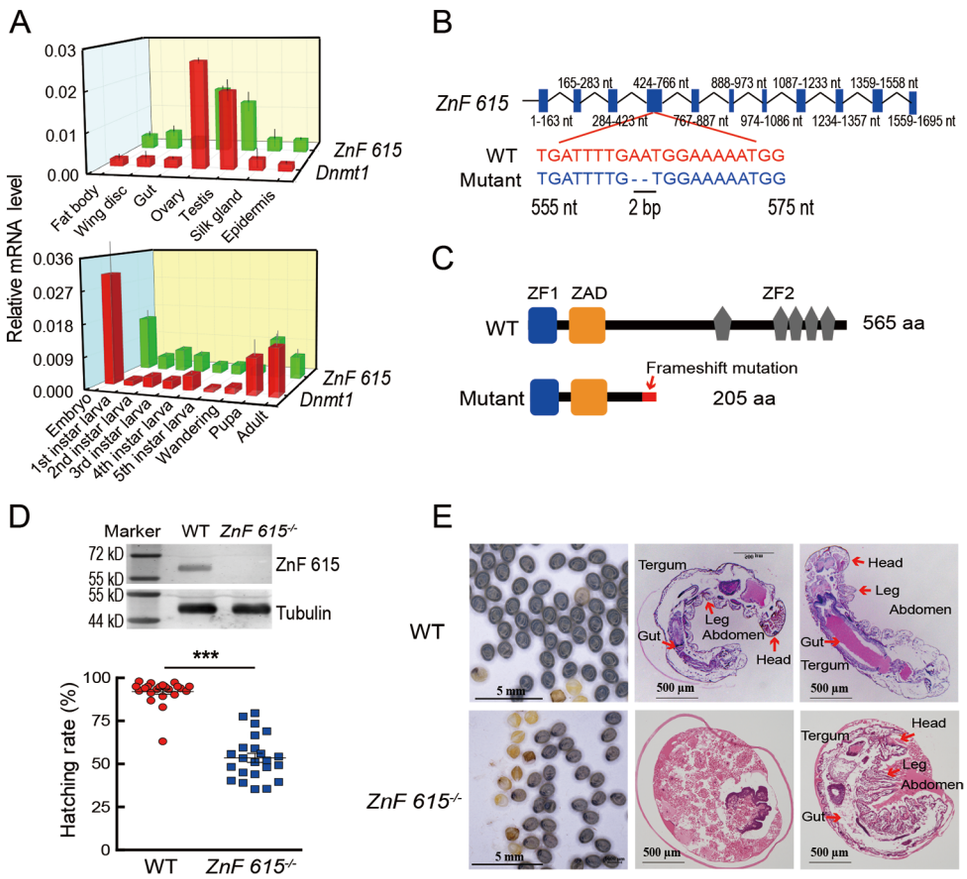

Figure 6 Loss-of-function analysis of *ZnF615* in *B. mori* embryos

A: Expression patterns of *Dnmt1* and *ZnF615* in different tissues, including epidermis, silk gland, testis, ovary, gut, wing disc, and fat body (top), and at different developmental stages, including embryo, 1st–5th instar larval, wandering larval, pupal, and adult stages (bottom). B: Schematic of nucleic acid base deletion site in *ZnF615* (top). C: Functional domain analysis of ZnF615 protein in WT and *ZnF615*$^{-/-}$ mutant. D: Western blot analysis of ZnF615 protein in WT and *ZnF615*$^{-/-}$ mutant embryos (top). Hatching rates in WT and *ZnF615*$^{-/-}$ mutant (bottom). Each point represents an embryo hatching rate of female WT or *ZnF615*$^{-/-}$ silkworms. E: Morphology and structure of WT and *ZnF615*$^{-/-}$ mutant embryos. Significant differences were determined by *t*-test (*: $P<0.05$; **: $P<0.01$; ***: $P<0.001$).

normally. We speculate that the defective Dnmt1 protein in the knockout mutant was still partially active after mutation, or the organism was able to activate other mechanisms to compensate for the damage caused by the lack of DNA methylation. These results highlight the necessity of *Dnmt1* expression and DNA methylation in early embryogenesis to ensure proper embryonic development in insects (Figure 1).

Importantly, in this study, we identified and characterized the nuclear protein gene *ZnF615*, which is modified by 5mC and acts downstream of *Dnmt1*. Here, *ZnF615* knockout resulted in embryo and ovary phenotypes similar to those of *Dnmt1* (Figure 6); moreover, 70% of the nutrient metabolism-related genes down-regulated by *Dnmt1* RNAi were regulated by *ZnF615* (Figure 7E; Supplementary Table S8), including lipid, amino acid, carbohydrate, and glycan metabolism-related pathways. Early embryonic development requires glycosidases to hydrolyze carbohydrates to produce glucose and provide energy; amino acids and fatty acids are also important for insect embryonic development (Levin et al., 2017). Knockdown of pancreatic lipase-related protein 2 in *Nilaparvata lugens* results in a decrease in the hatching rate (Xu et al., 2017). Thus, *Dnmt1* RNAi may impact insect development by affecting these few genes. *Dnmt1* RNAi inhibited *ZnF615* expression, leading to the down-regulation of genes required for embryogenesis. *Bombyx mori* ZnF615 is a typical C2H2 zinc finger protein; C2H2 zinc fingers comprise the most common and diverse family of transcription factors (Vaquerizas et al., 2009; Weirauch & Hughes, 2011; Wu et al., 2019). However, as the defective ZnF615 protein in knockout mutants contained a zinc finger motif and zinc finger associated domain and may be partially active, more than 50% of mutant embryos hatched normally.

In insects, 5mC occurs in genes with conserved housekeeping functions (Bonasio et al., 2012; Lyko et al., 2010; Sarda et al., 2012; Simola et al., 2013). Our WGBS and RNA-seq data revealed a positive correlation between high methylation rates and high expression levels of numerous housekeeping genes (Figure 2C; Supplementary Figure S4). However, *Dnmt1* RNAi did not down-regulate these housekeeping genes, as reported in other insects. For example, suppression of DNA methylation by *Dnmt1* RNAi in *Oncopeltus fasciatus* (Bewick et al., 2019) or by 5mC inhibitor

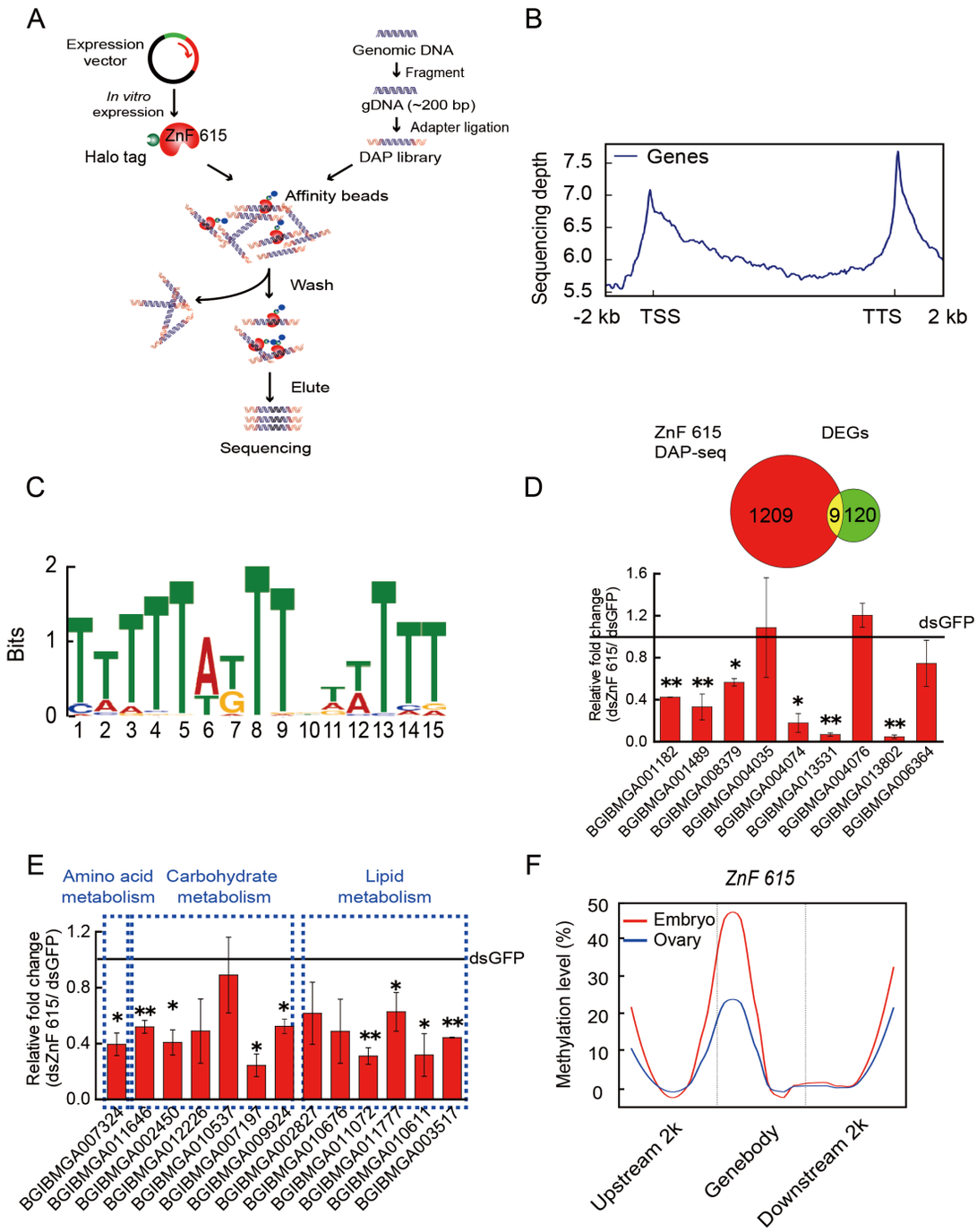

Figure 7 DAP-seq analysis of *ZnF615* in *B. mori* embryos

A: Overview of DAP-seq experimental process. cDNA of *ZnF615* ORF fused to Halo affinity tag was expressed *in vitro* and recombinant protein was bound to ligand-coupled beads. Genomic DNA at blastoderm stage of *B. mori* embryo was ultra-sonicated to 200 bp fragments, which were ligated with Illumina-based sequencing adaptors. HaloTag-ZnF615 protein was then incubated with adapter-ligated genomic DNA library. After unbound DNA fragments were washed away, the ZnF615-bound fragments were released. Released DNA fragments were then purified and sequenced. B: Peak frequency in different gene body regions between 2 kb upstream and downstream. C: Top-ranked motif in ZnF615 DAP-seq data was TTTTTATTGTTTTT. TSS: transcription start site; TTS: transcription termination site. Motifs were determined by MEME analysis using top-ranked peaks. D: Venn diagram comparing DEGs identified by RNA-seq after *Dnmt1* RNAi and *ZnF615* binding genes by DAP-Seq at blastoderm stage of embryo (top). Change in mRNA levels of genes both peak related and differentially expressed after *Dnmt1* RNAi in *ZnF615* RNAi *B. mori* embryos (bottom). E: Changes in mRNA levels of DEGs related to nutrient metabolism pathways enriched by *Dnmt1* RNAi in *ZnF615* RNAi *B. mori* embryos. F: Analysis of mCG levels and regions of *ZnF615* in *B. mori* ovary and blastoderm stage of embryo. Significance of results was determined by *t*-test (*: $P<0.05$; **: $P<0.01$).

treatment in *B. mori* (Xu et al., 2021) only down-regulates a small number of genes but has a significant impact on insect development. We previously speculated that highly expressed housekeeping genes may be regulated by multiple pathways or mechanisms, including DNA methylation (Xu et al., 2021). Therefore, the transcriptional inhibition caused by the loss of gene body methylation may be easily compensated by other regulatory pathways. Second, the transient loss of methylation caused by *Dnmt1* RNAi did not change the chromosomal structure of these genes, resulting in no change in gene expression.

In insects, 5mC usually occurs in the gene bodies of highly transcribed genes (Glastad et al., 2014; Wang et al., 2013; Xiang et al., 2010; Zemach et al., 2010) and does not inhibit transcription but leads to gene activation (Hellman & Chess, 2007; Meng et al., 2015; Wolf et al., 1984). This may occur because DNA methylation shapes chromatin and gene expression status by affecting the structure of nucleosomes and/or regulating other factors (Chodavarapu et al., 2010). In addition, methyl-CpG-binding proteins (MeCPs and MBDs) specifically recognize DNA methylation and change the local chromatin structure by recruiting histone-modifying enzymes or chromatin-remodeling complexes (Meng et al., 2015). Gene body methylation can also facilitate transcription elongation by inhibiting the activation of alternative promoters and controlling alternative splicing (Meng et al., 2015). In the *B. mori* ovaries, 5mC in the 5' regions of the gene bodies recruits acetyltransferase through MBD2/3 to enhance gene expression (Xu et al., 2021). Thus, consistent mechanisms of methylation targeting gene bodies (i.e., intragenic methylation) of protein metabolism-related genes may facilitate and promote embryogenesis. We demonstrated that Dnmt1 directly binds to the 5' region of the *ZnF615* gene body, thereby promoting its transcription efficiency by catalyzing 5mC formation (Figures 4, 5) and subsequent transcription of the *ZnF615* gene.

We found similar intragenic methylation enrichment in genes associated with protein metabolism-related pathways in the *B. mori* ovary (Xu et al., 2021) and embryo (Supplementary Figure S4). Furthermore, 5mC-modified *ZnF615* affected both ovarian and embryonic development by directly binding to protein metabolism-related genes and by indirectly regulating nutrient metabolism-related genes (Figures 2E, 7E; Supplementary Figure S4). The effect of 5mC-mediated *ZnF615* in ovarian and embryonic development was achieved through DNA methylation at the same *ZnF615* gene sites (Figure 7G). We revealed that, in insects, intragenic DNA methylation in the ovary can be inherited by the fertilized egg. In addition, the higher methylation levels of *ZnF615* in the embryos than in the ovaries (Figure 7G) may explain why Dnmt1 expression is up-regulated at the beginning of embryogenesis (Lyu et al., 2021). The up-regulation of DNA methylation in *ZnF615* enhanced its own expression and that of its downstream genes. Thus, the similar methylation patterns and levels in the ovary and embryo ensured the expression of embryogenesis-related genes.

In summary, this study demonstrated that intragenic DNA methylation enhances the expression of protein metabolism-related and nutrient metabolism-related genes through the DNA methyltransferase *Dnmt1* and transcription factor *ZnF615* to ensure ovarian and embryonic development, which may facilitate high fecundity in insects.

DATA AVAILABILITY

The raw Illumina sequencing data from WGBS of the *B. mori* early embryos were deposited in the NCBI Sequence Read Archive (SRA) under accession No. SRP343081 and GSA database under accession No. CRA006748. The raw Illumina sequencing data from RNA-seq after *Dnmt1* RNAi in *B. mori* embryos were deposited in the NCBI SRA under accession No. SRP342894 and GSA database under accession No. CRA006752. The raw Illumina sequencing data from DAP-seq were deposited in the NCBI SRA under accession No. SRP342920 and GSA database under accession No. CRA006730.

SUPPLEMENTARY DATA

Supplementary data to this article can be found online.

COMPETING INTERESTS

The authors declare that they have no competing interests.

AUTHORS' CONTRIBUTIONS

G.F.X. conducted most of the experiments, participated in data analyses, and drafted the manuscript. C.C.G., Y.L.T., T.Y.F., and Y.L.P. conducted *Dnmt1* and *ZnF615* knockout, egg number and hatch rate analysis, RNAi, gene cloning, and protein expression analysis. H.L., Y.G.L., and C.M.T. assisted with the experiments and insect rearing. Q.L.F. and Q.S.S. provided technical and material support, participated in discussions, and helped draft and revise the manuscript. S.C.Z. conceived the study design, supervised the study, and drafted and finalized the manuscript. All authors read and approved the final version of the manuscript.

ACKNOWLEDGMENTS

We would like to thank Professor Xiao-Qiang Yu and Associate Professor Liu Lin at South China Normal University, Guangzhou, China, for helpful discussions and comments on the article.

REFERENCES

Bartlett A, O'Malley RC, Huang SC, Galli M, Nery JR, Gallavotti A, et al. 2017. Mapping genome-wide transcription-factor binding sites using DAP-seq. *Nature Protocols*, **12**(8): 1659−1672.

Bewick AJ, Sanchez Z, Mckinney EC, Moore AJ, Moore PJ, Schmitz RJ. 2019. Dnmt1 is essential for egg production and embryo viability in the large milkweed bug. *Oncopeltus fasciatus. Epigenetics & Chromatin*, **12**(1): 6.

Bird A. 2002. DNA methylation patterns and epigenetic memory. *Genes & Development*, **16**(1): 6−21.

Boiani M, Eckardt S, Schöler HR, McLaughlin KJ. 2002. Oct4 distribution and level in mouse clones: consequences for pluripotency. *Genes & Development*, **16**(10): 1209−1219.

Bonasio R, Li QY, Lian JM, Mutti NS, Jin LJ, Zhao HM, et al. 2012. Genome-wide and caste-specific DNA methylomes of the ants *Camponotus floridanus* and *Harpegnathos saltator*. *Current Biology*, **22**(19): 1755–1764.

Bortvin A, Eggan K, Skaletsky H, Akutsu H, Berry DL, Yanagimachi R, et al. 2003. Incomplete reactivation of *Oct4*-related genes in mouse embryos cloned from somatic nuclei. *Development*, **130**(8): 1673−1680.

Byrne JA, Simonsson S, Western PS, Gurdon JB. 2003. Nuclei of adult mammalian somatic cells are directly reprogrammed to *oct-4* stem cell gene expression by amphibian oocytes. *Current Biology*, **13**(14): 1206−1213.

Chodavarapu RK, Feng SH, Bernatavichute YV, Chen PY, Stroud H, Yu YC, et al. 2010. Relationship between nucleosome positioning and DNA methylation. *Nature*, **466**(7304): 388−392.

Dos Santos Mendonça A, Silveira MM, Rios ÁFL, Mangiavacchi PM, Caetano AR, Dode MAN, et al. 2019. DNA methylation and functional characterization of the XIST gene during *in vitro* early embryo development in cattle. *Epigenetics*, **14**(6): 568−588.

Falckenhayn C, Boerjan B, Raddatz G, Frohme M, Schoofs L, Lyko F. 2013. Characterization of genome methylation patterns in the desert locust *Schistocerca gregaria*. *Journal of Experimental Biology*, **216**(8): 1423–1429.

Feliciello I, Parazajder J, Akrap I, Ugarković Đ. 2013. First evidence of DNA methylation in insect *Tribolium castaneum*: environmental regulation of DNA methylation within heterochromatin. *Epigenetics*, **8**(5): 534−541.

Glastad KM, Hunt BG, Goodisman MAD. 2014. Evolutionary insights into DNA methylation in insects. *Current Opinion in Insect Science*, **1**: 25−30.

Glastad KM, Hunt BG, Yi SV, Goodisman MAD. 2011. DNA methylation in insects: on the brink of the epigenomic era. *Insect Molecular Biology*, **20**(5): 553−565.

Greenberg MVC, Bourc'his D. 2019. The diverse roles of DNA methylation in mammalian development and disease. *Nature Reviews Molecular Cell Biology*, **20**(10): 590−607.

Hellman A, Chess A. 2007. Gene body-specific methylation on the active X chromosome. *Science*, **315**(5815): 1141−1143.

Khurad AM, Zhang MJ, Deshmukh CG, Bahekar RS, Tiple AD, Zhang CX. 2009. A new continuous cell line from larval ovaries of silkworm. *Bombyx mori*. *In Vitro Cellular & Developmental Biology-Animal*, **45**(8): 414−419.

Kim D, Langmead B, Salzberg SL. 2015. HISAT: a fast spliced aligner with low memory requirements. *Nature Methods*, **12**(4): 357−360.

Langmead B, Salzberg SL. 2012. Fast gapped-read alignment with Bowtie 2. *Nature Methods*, **9**(4): 357−359.

Levin E, McCue MD, Davidowitz G. 2017. More than just sugar: allocation of nectar amino acids and fatty acids in a Lepidopteran. *Proceedings of the Royal Society B:Biological Sciences*, **284**(1848): 20162126.

Li B, Hu P, Zhu LB, You LL, Cao HH, Wang J, et al. 2020. DNA methylation is correlated with gene expression during diapause termination of early embryonic development in the silkworm (*Bombyx mori*). *International Journal of Molecular Sciences*, **21**(2): 671.

Lister R, Pelizzola M, Dowen RH, Hawkins RD, Hon G, Tonti-Filippini J, et al. 2009. Human DNA methylomes at base resolution show widespread epigenomic differences. *Nature*, **462**(7271): 315−322.

Livak KJ, Schmittgen TD. 2001. Analysis of relative gene expression data using real-time quantitative PCR and the 2-ΔΔCT method. *Methods*, **25**(4): 402−408.

Love MI, Huber W, Anders S. 2014. Moderated estimation of fold change and dispersion for RNA-seq data with DESeq2. *Genome Biology*, **15**(12): 550.

Lyko F, Foret S, Kucharski R, Wolf S, Falckenhayn C, Maleszka R. 2010. The honey bee epigenomes: differential methylation of brain DNA in queens and workers. *PLoS Biology*, **8**(11): e1000506.

Lyko F, Maleszka R. 2011. Insects as innovative models for functional studies of DNA methylation. *Trends in Genetics*, **27**(4): 127−131.

Lyu H, Xu GF, Peng XZ, Gong CC, Peng YL, Song QS, et al. 2021. Interacting C/EBPg and YBP regulate DNA methyltransferase 1 expression in *Bombyx mori* embryos and ovaries. *Insect Biochemistry and Molecular Biology*, **134**: 103583.

Meng H, Cao Y, Qin JZ, Song XY, Zhang Q, Shi Y, et al. 2015. DNA methylation, its mediators and genome integrity. *International Journal of Biological Sciences*, **11**(5): 604−617.

Naito Y, Hino K, Bono H, Ui-Tei K. 2015. CRISPRdirect: software for designing CRISPR/Cas guide RNA with reduced off-target sites. *Bioinformatics*, **31**(7): 1120−1123.

Ramírez F, Ryan DP, Grüning B, Bhardwaj V, Kilpert F, Richter AS, et al. 2016. deepTools2: a next generation web server for deep-sequencing data analysis. *Nucleic Acids Research*, **44**(W1): W160−W165.

Razin A, Riggs AD. 1980. DNA methylation and gene function. *Science*, **210**(4470): 604−610.

Rishi V, Bhattacharya P, Chatterjee R, Rozenberg J, Zhao JF, Glass K, et al. 2010. CpG methylation of half-CRE sequences creates C/EBPα binding sites that activate some tissue-specific genes. *Proceedings of the National Academy of Sciences of the United States of America*, **107**(47): 20311−20316.

Sarda S, Zeng J, Hunt BG, Yi SV. 2012. The Evolution of invertebrate gene body methylation. *Molecular Biology and Evolution*, **29**(8): 1907−1916.

Simola DF, Wissler L, Donahue G, Waterhouse RM, Helmkampf M, Roux J, et al. 2013. Social insect genomes exhibit dramatic evolution in gene composition and regulation while preserving regulatory features linked to sociality. *Genome Research*, **23**(8): 1235−1247.

Simonsson S, Gurdon J. 2004. DNA demethylation is necessary for the epigenetic reprogramming of somatic cell nuclei. *Nature Cell Biology*, **6**(10): 984−990.

Slieker RC, Roost MS, van Iperen L, Suchiman HED, Tobi EW, Carlotti F, et al. 2015. DNA methylation landscapes of human fetal development. *PLoS Genetics*, **11**(10): e1005583.

Smith ZD, Chan MM, Humm KC, Karnik R, Mekhoubad S, Regev A, et al. 2014. DNA methylation dynamics of the human preimplantation embryo. *Nature*, **511**(7511): 611−615.

Takebayashi SI, Tamura T, Matsuoka C, Okano M. 2007. Major and essential role for the DNA methylation mark in mouse embryogenesis and stable association of DNMT1 with newly replicated regions. *Molecular and Cellular Biology*, **27**(23): 8243−8258.

Trapnell C, Roberts A, Goff L, Pertea G, Kim D, Kelley DR, et al. 2012. Differential gene and transcript expression analysis of RNA-seq experiments with TopHat and Cufflinks. *Nature Protocols*, **7**(3): 562−578.

Vaquerizas JM, Kummerfeld SK, Teichmann SA, Luscombe NM. 2009. A census of human transcription factors: function, expression and evolution. *Nature Reviews Genetics*, **10**(4): 252−263.

Ventós-Alfonso A, Ylla G, Montañes JC, Belles X. 2020. DNMT1 promotes genome methylation and early embryo development in cockroaches. *iScience*, **23**(12): 101778.

Wang J, Xia QY, He XM, Dai MT, Ruan J, Chen J, et al. 2005. SilkDB: a knowledgebase for silkworm biology and genomics. *Nucleic Acids Research*, **33**: D399−D402.

Wang X, Wheeler D, Avery A, Rago A, Choi JH, Colbourne JK, et al. 2013.

Function and evolution of DNA methylation in Nasonia vitripennis. *PLoS Genetics*, **9**(10): e1003872.

Weirauch MT, Hughes TR. 2011. A catalogue of eukaryotic transcription factor types, their evolutionary origin, and species distribution. *Subcellular Biochemistry*, **52**: 25−73.

Werren JH, Richards S, Desjardins CA, Niehuis O, Gadau J, Colbourne JK, et al. 2010. Functional and evolutionary insights from the genomes of three parasitoid *Nasonia* species. *Science*, **327**(5963): 343−348.

Wolf SF, Jolly DJ, Lunnen KD, Friedmann T, Migeon BR. 1984. Methylation of the hypoxanthine phosphoribosyltransferase locus on the human X chromosome: implications for X-chromosome inactivation. *Proceedings of the National Academy of Sciences of the United States of America*, **81**(9): 2806−2810.

Wu SY, Tong XL, Li CL, Lu KP, Tan D, Hu H, et al. 2019. Genome-wide identification and expression profiling of the C2H2-type zinc finger protein genes in the silkworm *Bombyx mori*. *PeerJ*, **7**: e7222.

Xi YX, Li W. 2009. BSMAP: whole genome bisulfite sequence MAPping program. *BMC Bioinformatics*, **10**: 232.

Xia QY, Zhou ZY, Lu C, Cheng DJ, Dai FY, Li B, et al. 2004. A draft sequence for the genome of the domesticated silkworm (*Bombyx mori*). *Science*, **306**(5703): 1937−1940.

Xiang H, Li X, Dai FY, Xu X, Tan AJ, Chen L, et al. 2013. Comparative methylomics between domesticated and wild silkworms implies possible epigenetic influences on silkworm domestication. *BMC Genomics*, **14**: 646.

Xiang H, Zhu JD, Chen Q, Dai FY, Li X, Li MW, et al. 2010. Single base-resolution methylome of the silkworm reveals a sparse epigenomic map. *Nature Biotechnology*, **28**(5): 516−520.

Xu GF, Gong CC, Lyu H, Deng HM, Zheng SC. 2022a. Dynamic transcriptome analysis of *Bombyx mori* embryonic development. *Insect Science*, **29**(2): 344−362.

Xu GF, Lyu H, Yi YQ, Peng YL, Feng QL, Song QS, et al. 2021. Intragenic DNA methylation regulates insect gene expression and reproduction through the MBD/Tip60 complex. *iScience*, **24**(2): 102040.

Xu GF, Tian YL, Peng YL, Zheng SC. 2022b. Knock down of target genes by RNA interference in the embryos of lepidopteran insect. *Bombyx mori. STAR Protocols*, **3**(1): 101219.

Xu GF, Yi YQ, Lyu H, Gong CC, Feng QL, Song QS, et al. 2020. DNA methylation suppresses chitin degradation and promotes the wing development by inhibiting Bmara-mediated chitinase expression in the silkworm. *Bombyx mori. Epigenetics & Chromatin*, **13**(1): 34.

Xu GF, Zhang J, Lyu H, Song QS, Feng QL, Xiang H, et al. 2018. DNA methylation mediates BmDeaf1-regulated tissue- and stage-specific expression of *BmCHSA-2b* in the silkworm. *Bombyx mori. Epigenetics & Chromatin*, **11**(1): 32.

Xu L, Huang HJ, Zhou X, Liu CW, Bao YY. 2017. Pancreatic lipase-related protein 2 is essential for egg hatching in the brown planthopper. *Nilaparvata lugens*. *Insect Molecular Biology*, **26**(3): 277−285.

Yan H, Bonasio R, Simola DF, Liebig J, Berger SL, Reinberg D. 2015. DNA methylation in social insects: how epigenetics can control behavior and longevity. *Annual Review of Entomology*, **60**: 435−452.

Yu GC, Wang LG, He QY. 2015. ChIPseeker: an R/Bioconductor package for ChIP peak annotation, comparison and visualization. *Bioinformatics*, **31**(14): 2382−2383.

Zemach A, McDaniel IE, Silva P, Zilberman D. 2010. Genome-wide evolutionary analysis of eukaryotic DNA methylation. *Science*, **328**(5980): 916−919.

Zhang Y, Liu T, Meyer CA, Eeckhoute J, Johnson DS, Bernstein BE, et al. 2008. Model-based analysis of ChIP-Seq (MACS). *Genome Biology*, **9**(9): R137.

Zilberman D. 2008. The evolving functions of DNA methylation. *Current Opinion in Plant Biology*, **11**(5): 554−559.

Zwier MV, Verhulst EC, Zwahlen RD, Beukeboom LW, van de Zande L. 2012. DNA methylation plays a crucial role during early *Nasonia* development. *Insect Molecular Biology*, **21**(1): 129−138.